

# Clustering Constraints on the Relative Sizes of Central and Satellite Galaxies

Andrew Hearin<sup>1</sup>, Peter Behroozi<sup>2</sup>, Andrey Kravtsov<sup>3</sup>, Benjamin Moster<sup>4</sup>

<sup>1</sup>*Argonne National Laboratory, Argonne, IL, USA 60439, USA*

<sup>2</sup>*Department of Physics, University of Arizona, 1118 E 4th St, Tucson, AZ 85721 USA*

<sup>3</sup>*Department of Astronomy & Astrophysics, The University of Chicago, Chicago, IL 60637 USA*

<sup>4</sup>*Universitäts-Sternwarte, Ludwig-Maximilians-Universität München, Scheinerstr. 1, 81679 München, Germany*

2 November 2017

## ABSTRACT

We place empirical constraints on the connection between dark matter halos and galaxy half-light radii,  $R_{1/2}$ . Low-redshift SDSS measurements show that smaller galaxies cluster much more strongly than larger galaxies at fixed stellar mass. Using `Halotools` to forward model the observations, we find that the clustering signal generically requires satellite galaxies to be smaller than central galaxies of the same halo mass. We present a simple empirical model consistent with the clustering results, in which galaxy size is proportional to halo virial radius at the time of peak halo mass. We use this model to predict how galaxy lensing,  $\Delta\Sigma$ , should depend on  $R_{1/2}$  for  $M_*$ -complete samples. Other simple empirical models fail the clustering test, such as models in which galaxy size is related to stellar mass alone; these failures persist even when accounting for possible effects from satellite stripping and orphan galaxies. Our results suggest that the relative size of centrals and satellites is predetermined at the time of satellite infall, and that a remarkably simple galaxy–halo scaling relation emerges from the complex physics regulating galaxy size.

## 1 INTRODUCTION

In the  $\Lambda$ CDM framework of cosmological structure formation, galaxies form at the centers of dark matter halos. Highly complex and nonlinear baryonic processes regulate galaxy formation, and the quest for a fine-grained understanding of these processes is one of the chief goals of theoretical astrophysics today.

Observationally, many properties of observed galaxies exhibit remarkably tight scaling relations. Among the most fundamental of these relations is the strong correlation between galaxy size and stellar mass and luminosity. The scaling of galaxy size with galaxy mass is well-measured in the local Universe (Shen et al. 2003; Guo et al. 2009; Huang et al. 2013; Zhang & Yang 2017) and at high-redshift (Trujillo et al. 2004; van der Wel et al. 2014; Kawamata et al. 2015; Shibuya et al. 2015; Huertas-Company et al. 2013; Lange et al. 2015; Huang et al. 2017).

These well-measured scaling relations are challenging to faithfully recover using ab initio galaxy formation methods such as hydrodynamical simulations and semi-analytic models, and provide useful boundary conditions for the calibration of such modeling efforts (Khochfar & Silk 2006; Dutton et al. 2011; Hopkins et al. 2010; Bottrell et al. 2017). The precision cosmology program also depends critically on accurate modeling of galaxies, so that cosmological parameter inference can be confidently

conducted without undue interference from uncertainty in baryonic physics (LSST Science Collaboration et al. 2009; Robertson et al. 2017).

## 2 DATA AND SIMULATIONS

Our galaxy sample comes from the catalog of SDSS galaxy profile decompositions provided by Meert et al. (2015). This catalog is based on Data Release 10 of the Sloan Digital Sky Survey (SDSS, Ahn et al. 2014), with improvements to the photometry pipeline and light profile fitting methods (Vikram et al. 2010; Bernardi et al. 2013, 2014; Meert et al. 2013). In the version of this catalog that we use, two-dimensional  $r$ -band profiles were fit with a two-component de Vaucouleurs + exponential profile to determine the half-light radius  $R_{1/2}$ . We use stellar mass measurements made available through the MPA-JHU catalog (Kauffmann et al. 2003; Brinchmann et al. 2004), allowing us to define volume-limited samples of galaxies according to the same completeness cuts used in Behroozi et al. (2015) (see Figure 2).

We calculate two-point clustering  $w_p$  of our SDSS galaxy sample using line-of-sight projection of  $\pi_{\max} = 20\text{Mpc}$  using the `correl` program in `UniverseMachine`. **PSB: Please fill in details about `correl` here.**

As the bedrock of our modeling, we use the pub-

licly available<sup>1</sup> catalog of **Rockstar** subhalos identified at  $z = 0$  in the Bolshoi-Planck simulation (Klypin et al. 2011; Behroozi et al. 2013,?; Riebe et al. 2013; Rodríguez-Puebla et al. 2016). As described in §3.1, we will use traditional abundance matching to connect stellar mass  $M_*$  with subhalo peak mass  $M_{\text{peak}}$ . To address issues related to subhalo incompleteness (Guo & White 2014), we supplement the Bolshoi-Planck subhalo catalog with *all* subhalos that were ever identified by **Rockstar**, including those that no longer appear in the standard catalog as subhalos that survive to  $z = 0$ . We describe our treatment of these “orphan” subhalos in the Appendix.

For mock galaxies, to compute galaxy clustering we employ the distant observer approximation by treating the simulation  $z$ -axis as the line-of-sight. We compute  $w_p$  using the `mock_observables.wp` function in **Halotools**, which is a python implementation of the algorithm in the **Corrfunc** C library (Sinha & Garrison 2017).

All numerical values of  $R_{1/2}$  will be quoted in physical kpc, and all values of  $M_*$  and  $M_{\text{halo}}$  in  $M_\odot$ , assuming  $H_0 = 67.8 \text{ km/s} \equiv 100h \text{ km/s}$ , the best-fit value from Planck Collaboration et al. (2016). To scale stellar masses to “ $h = 1$  units” (Croton 2013), our numerically quoted values for  $M_*$  should be multiplied by a factor of  $h^2$ , while our halo masses and distances should be multiplied by a factor of  $h$ .

## 2.1 Classifying large vs. small galaxies

Because galaxy clustering has well-known dependence upon  $M_*$  that is not the subject of this work, we wish to remove this influence and focus purely on the relationship between  $R_{1/2}$  and  $w_p(r_p)$ . To do so, we determine the value  $\langle R_{1/2} | M_* \rangle$  by computing a sliding median of  $R_{1/2}$ , calculated using a window of width  $N_{\text{gal}} = 1000$ . Each galaxy is categorized as either “large” or “small” according to whether it is above or below the median value appropriate for its stellar mass. Using this technique, we stress that for any  $M_*$ -threshold sample, the SMF of the “large” and “small” subsamples are identical, by construction. See Figure 1.

## 3 GALAXY-HALO MODEL

### 3.1 Abundance Matching

We map  $M_*$  onto subhalos using deconvolution abundance matching on the orphan-supplemented Bolshoi-Planck subhalo catalog, as described in detail in the Appendix. Briefly, our abundance matching prescription is based  $M_{\text{peak}}$ , the largest value of  $M_{\text{vir}}$  ever attained along the main progenitor branch of the subhalo.

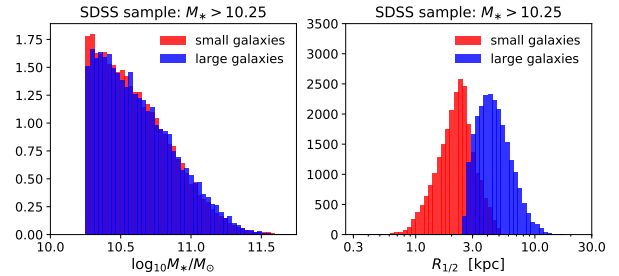


**Figure 1. Definition of “small” and “large” galaxies.** For a volume-limited SDSS galaxy sample defined by  $M_* > 10^{10.25} M_\odot$ , we visually demonstrate how we classify galaxies into “small” and “large” subsamples. As described in detail in §2.1, we compute the median value  $\langle R_{1/2} | M_* \rangle_{\text{median}}$  using a sliding window with a width of 1000 galaxies at each value of  $M_*$ . The *left panel* shows a histogram of the stellar masses, confirming that our method yields identical stellar mass functions for the two subsamples. The *right panel* shows histograms of  $R_{1/2}$  for the two subsamples, which partially overlap due to the finite range of  $M_*$  in the volume-limited sample.

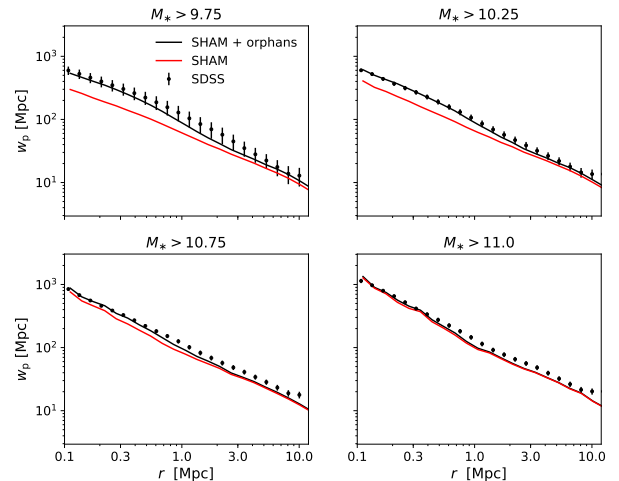


**Figure 2. SHAM + orphan clustering predictions.** Using the abundance matching methods described in §??, we compare the projected clustering of mock vs. SDSS galaxies. Each panel shows the comparison for a volume-limited sample defined by a different  $M_*$ -threshold. Black points with error bars show SDSS measurements; solid red (black) curves show the abundance matching prediction including (excluding) the effect of orphan subhalos (see Appendix A). Including orphans mitigates the discrepancy in the clustering predicted by traditional,  $M_{\text{peak}}$ -based SHAM based, though mild tension remains for  $M_* \gtrsim 10^{10.75} M_\odot$ .

### 3.2 Galaxy size models

In §4, we calculate predictions for the  $R_{1/2}$ -dependence of galaxy clustering for several different kinds of empirical models, described in turn below.

#### 3.2.1 $M_*$ -based model

In the first class of models we explore, we suppose that stellar mass  $M_*$  is the statistical regulator of  $R_{1/2}$ , so that

<sup>1</sup> [http://www.slac.stanford.edu/~behroozi/BPlanck\\_Hlists](http://www.slac.stanford.edu/~behroozi/BPlanck_Hlists)

galaxy sizes are drawn from a log-normal distribution centered at  $\langle R_{1/2}|M_* \rangle_{\text{median}}$ . To implement this model, for simplicity we directly tabulate  $\langle R_{1/2}|M_* \rangle_{\text{median}}$  directly from the data, rather than pursue a parametric form (see, e.g., Zhang & Yang 2017).

### 3.2.2 $R_{\text{vir}}$ -based model

Motivated by Kravtsov (2013), we explore a model in which  $R_{1/2}$  is linearly proportional to halo virial radius:

$$R_{1/2} = 0.01 R_{\text{vir}} \quad (1)$$

For the virial radius of halos and subhalos, we use  $R_{\text{Mpeak}}$ , the value of  $R_{\text{vir}}$  in physical units of kpc measured at the time of peak subhalo mass, defined by

$$M_{\text{peak}} \equiv \frac{4\pi}{3} R_{\text{Mpeak}}^3 \Delta_{\text{vir}}(z_{\text{Mpeak}}) \rho_{\text{m}}(z_{\text{Mpeak}}), \quad (2)$$

where for  $\Delta_{\text{vir}}(z_{\text{Mpeak}})$  we use the fitting function to the “virial” definition used in Bryan & Norman (1998). For the model we refer to as the “ $R_{\text{vir}}$ -based model”, we add uncorrelated log-normal scatter of  $\sigma_{R_{1/2}} = 0.2$  dex to generate a Monto Carlo realization of the model population.

### 3.2.3 $M_*$ -stripping model

As we will show in §4, the chief ingredient needed to recover the observed clustering properties of galaxies is that satellites need to be smaller than centrals of comparable halo mass. Thus it is natural to consider a class of models in which stellar mass is stripped from satellite galaxies after infall.

The basis of this class of models is the fitting function presented in Smith et al. (2016), which was calibrated by studying stellar mass loss in a suite of high-resolution hydrodynamical simulations. In this model,  $f_*$  quantifies the fraction of stellar mass lost as a function of  $f_{\text{DM}}$ , the amount of dark matter that has been stripped since infall:

$$f_* = 1 - \exp(-14.2 f_{\text{DM}}) \quad (3)$$

For  $f_{\text{DM}}$  we use the ratio of present-day subhalo mass divided by the peak mass,  $M_{\text{vir}}/M_{\text{peak}}$ . If we denote the post-stripping stellar mass as  $M'_*$ , then we have  $M'_* \equiv f_* M_*$ , where  $M_*$  is given by Eq. ???. We then calculate the post-stripping radius by interpolating  $\langle R_{1/2}|M'_* \rangle$  directly from SDSS data.

## 4 RESULTS

### 4.1 Size-Mass Scaling Relation

In Figure 3 we show the scaling of galaxy size  $R_{1/2}$  with  $M_*$ . The black curve enveloped by the gray bands show the scaling relation for SDSS galaxies, while the blue curve shows the median relation  $\langle R_{1/2}|M_* \rangle_{\text{median}}$  implied by the  $R_{\text{vir}}$ -based model described in §3. This figure shows that models in which  $R_{1/2} \propto R_{\text{vir}}$  can naturally give rise to the characteristic curvature in the  $\langle R_{1/2}|M_* \rangle$  relation, confirming the results in Kravtsov (2013) in a forward modeling context.

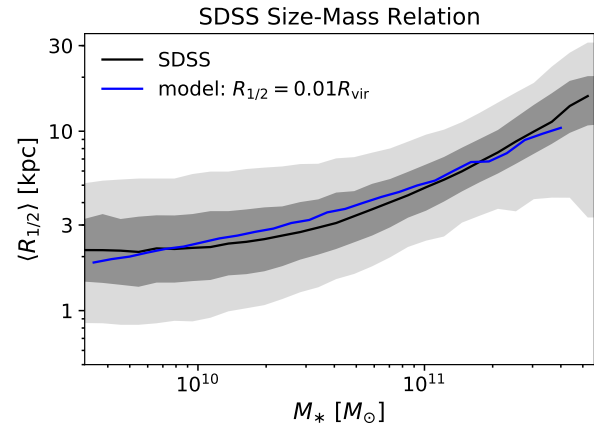


**Figure 3.** The black curve shows the median size-mass relation of SDSS galaxies as measured in Meert et al. (2015). The two gray bands enveloping the black curve show the 50% and 90% percentile regions. The blue curve shows  $R_{\text{vir}}$ -based model in which  $\langle R_{1/2}|R_{\text{vir}} \rangle_{\text{median}} = 0.01 R_{\text{vir}}$ . This figure confirms that a linear relationship between  $R_{\text{vir}}$  and  $R_{1/2}$ , convolved against the nonlinear relationships between  $R_{\text{vir}}$ ,  $M_{\text{halo}}$  and  $M_*$ , predicts the characteristic curvature in the relation  $\langle R_{1/2}|M_* \rangle_{\text{median}}$  over a wide range in mass.

### 4.2 Size-Dependent Clustering

In Figure 5 we present new measurements of the  $R_{1/2}$ -dependence of projected galaxy clustering,  $w_p(r_p)$ .

We measure  $w_p(r_p)$  separately for large and small subsamples for four different  $M_*$  thresholds,  $M_* > 10^{9.75} M_\odot$ ,  $M_* > 10^{10.25} M_\odot$ ,  $M_* > 10^{10.75} M_\odot$ , and  $M_* > 10^{11} M_\odot$ . We make the same measurements for each volume-limited  $M_*$ -threshold sample *without* splitting on size, giving us measurements  $w_p^{\text{all}}$ ,  $w_p^{\text{large}}$ , and  $w_p^{\text{small}}$  for each threshold sample. This allows us to compute the ratio  $(w_p^{\text{large}} - w_p^{\text{small}})/w_p^{\text{all}}$ , which we refer to as the  $R_{1/2}$  clustering ratio. These ratios are the measurements appearing on the y-axis in each panel of Figure 5. Points with jackknife-estimated error bars show SDSS measurements, solid curves show the clustering ratios of model galaxies as predicted by the models described in §3.

The salient feature of the clustering ratio measurements is that they are negative: small galaxies cluster more strongly than large galaxies of the same stellar mass. This feature also holds true for galaxies predicted by the  $R_{\text{vir}}$ -based model. This result may be surprising, since  $R_{1/2} \propto R_{\text{vir}}$ , halo mass  $R_{\text{vir}} \propto M_{\text{halo}}^{1/3}$ , and clustering strength increases with  $M_{\text{vir}}$ . Based on this simple argument, one would expect the opposite trend to the measurements shown here.

### 4.3 Central vs. Satellite Sizes

A straightforward resolution to the above puzzle is shown in Figure 6, which compares the  $R_{1/2}$  distributions of central, satellite, and splashback galaxies with the same halo mass  $M_{\text{peak}} \approx 10^{12} M_\odot$ . A “splashback” galaxy is defined as a present-day central that used to be a satellite, i.e., its main progenitor halo passed inside the virial radius of a larger halo at some point in its past history. On the

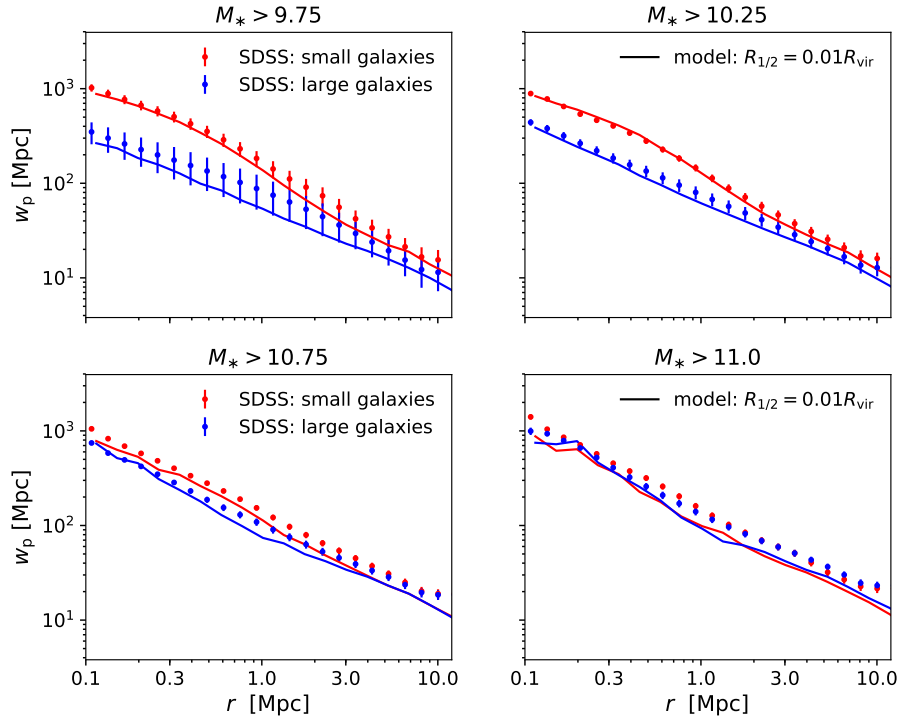


**Figure 4.**  $R_{1/2}$ –dependence of galaxy clustering. Red and blue points with error bars show our SDSS measurements of the clustering of small and large galaxies, respectively. For each volume-limited sample of  $M_*$ –complete galaxies, the small and large subsamples have identical stellar mass functions, as shown in Figure 1. Small galaxies cluster much more strongly relative to large galaxies of the same stellar mass. Solid curves show the clustering predictions of the  $R_{\text{vir}}$ –based model described in §3.2.2. The  $R_{\text{vir}}$ –based model inherits the shortcoming of ordinary abundance matching at  $M_* \gtrsim 10^{10.75} M_\odot$ , although the model faithfully captures the *relative* clustering of small vs. large galaxies, as shown in Figure 5.

other hand, we define a “true central” as a galaxy that has never been a satellite.

In the  $R_{\text{vir}}$ –based model, satellite and splashback galaxies are smaller than centrals of the same halo mass due to the physical size of their halo being smaller at earlier times  $z_{M_{\text{peak}}}$ . There are two distinct reasons why this feature results in small galaxies being more strongly clustered relative to larger galaxies of the same mass. First, satellite galaxies statistically occupy higher mass host halos that are more strongly clustered. In models where satellites are smaller than centrals, for any given  $M_*$ –threshold the “small” subsample will naturally have a higher satellite fraction, resulting in a negative clustering ratio as seen in SDSS data. Second, at fixed mass, halos of  $L_*$  galaxies that form earlier are more strongly clustered, a phenomenon commonly known as *halo assembly bias*. Since splashback halos are typically earlier forming than true centrals, then models where splashback halos host smaller-than-average galaxies will naturally predict negative clustering ratios.

In the  $M_*$ –based model, in which  $R_{1/2}$  is statistically set by present-day stellar mass with no other dependencies. Thus neither of the above features are present: satellites and centrals of the same mass have no differences in size, and there is essentially no  $R_{1/2}$ –dependence to galaxy clustering, in gross disagreement with our SDSS observations.

#### 4.4 Failure of $M_*$ –based Models

We conclude this section with a discussion of Figure 9, which provides an estimate of how satellite mass stripping and orphan galaxies impact size-dependent clustering ratios. In the  $M_*$ –stripping model described in §3.2.3, satellites lose stellar mass in a way that mimics what is seen in high-resolution hydrodynamical simulations. This naturally results in an enhancement of size differences between satellites and centrals, and the dot-dashed curves in Figure 9 show that produces the expected sign of the effect on the clustering ratios. The magnitude of the effect, however is not strong enough to remedy the discrepancy of the clustering predictions of the  $M_*$ –based model. We discuss the physical implications of this result in §5.3.

The dotted curves in Figure 9 show results of the  $R_{\text{vir}}$ –based model applied to a subhalo catalog that includes an orphan halos. As described in §??, orphan halos are subhalos that are no longer resolved by *Rockstar*, but whose evolution is tracked in a post-processing phase. We apply the same mass-stripping model described in §3.2.3 to this subhalo catalog that includes orphan halos, keep all model galaxies that retain more than half of their stellar mass, and show results for the  $R_{\text{vir}}$ –based model applied to the resulting catalog.

As the orphan catalog has a higher satellite fraction than the standard subhalo catalog, the negative boost shown the dotted curves in Figure 9 is expected. Orphan

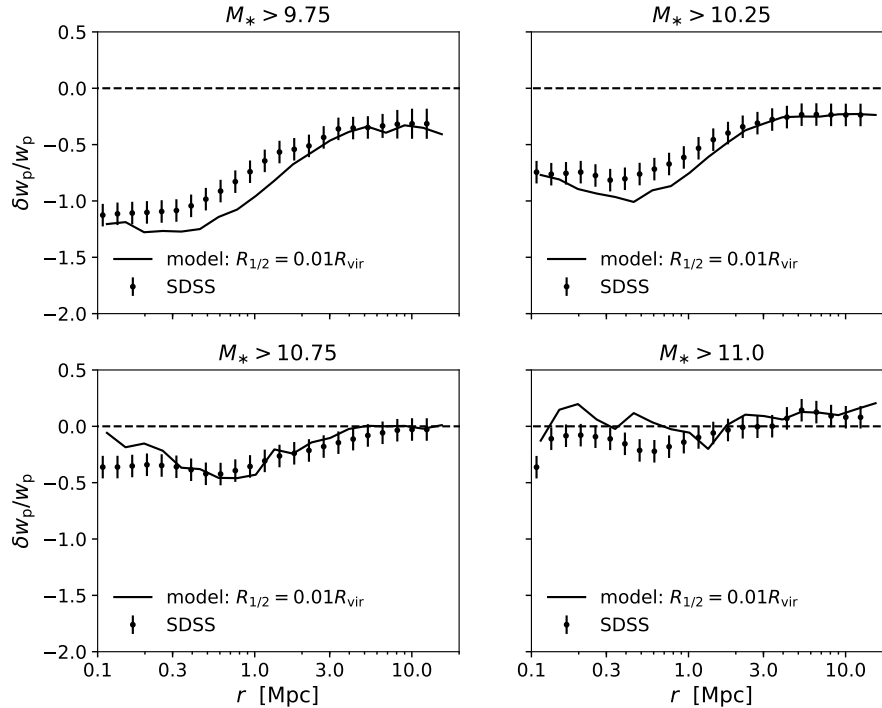


**Figure 5.  $R_{1/2}$ -dependence of galaxy clustering: clustering ratios.** Closely related to Figure 4, the y-axes show *clustering strength ratios*, defined as  $(w_p^{\text{large}} - w_p^{\text{small}})/w_p^{\text{all}}$ . Thus a y-axis value of  $-0.5$  corresponds to small galaxies being 50% more strongly clustered than large galaxies of the same stellar mass. Solid curves show the clustering ratio predictions of the  $R_{\text{vir}}$ -based model described in §3.2.2. Normalizing the measurements and predictions by  $w_p^{\text{all}}$  scales away the shortcoming of ordinary abundance matching at high stellar mass (see Figure 2), highlighting the successful prediction of the  $R_{\text{vir}}$ -based model for the  $R_{1/2}$ -dependence of galaxy clustering.

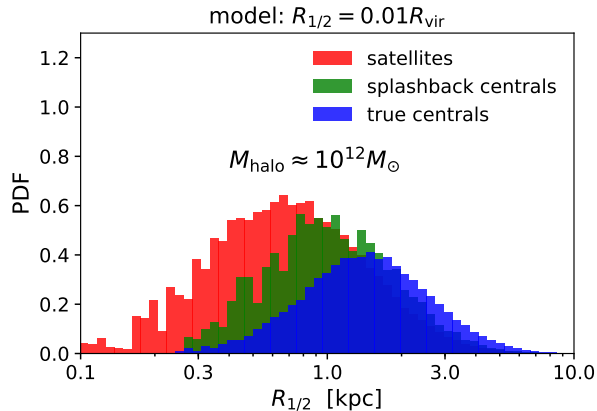


**Figure 6. Relative sizes of centrals and satellites.** In a narrow bin of halo mass  $M_{\text{halo}} \equiv M_{\text{peak}} \approx 10^{12} M_{\odot}$ , we show the distribution of model galaxy sizes for different subpopulations galaxies, as predicted by the  $R_{\text{vir}}$ -based model. The red histogram shows the sizes of satellites; the blue histogram shows host halos that have never passed inside the virial radius of a larger halo (“true centrals”); the green histogram host halos that were subhalos inside a larger at some point in their past history (“splashback centrals”). In the  $R_{\text{vir}}$ -based model, galaxy size is set by the *physical* size of the virial radius at the time the halo attains its peak mass, naturally resulting in smaller sizes for satellites and splashback centrals relative to true centrals of the same  $M_{\text{halo}}$ .

halos also typically have earlier-than-average values of  $z_{M_{\text{peak}}}$  relative to ordinary subhalos, which also enhances differences between central and satellite sizes. See §5.3 for further discussion.

#### 4.5 The Role of Morphology and Color

### 5 DISCUSSION

#### 5.1 Progression from Backwards to Forward Modeling

Our results give an archetypal demonstration of the natural scientific progression from backwards to forward modeling. In backwards modeling, some mapping is applied to observed galaxies to estimate the values of model quantities such as halo mass. In Kravtsov (2013), the model quantities mapped onto galaxies are  $M_{\text{halo}}$  and  $R_{\text{vir}}$ ; another classic example of backwards modeling uses a group- or cluster-finding algorithm to assign  $M_{\text{halo}}$  to observed galaxies (e.g., Berlind et al. 2006; Yang et al. 2005; Rykoff et al. 2014). Once the observed galaxies have been supplemented with model variables, then the relations of the galaxy-halo connection can be inferred, for example, by calculating quantities such as the mean stellar mass or quiescent fraction as a function of halo mass (e.g., Yang et al. 2005; Weinmann et al. 2006).

In forward modeling, the direction of inference is turned around: a mapping is instead applied to the model



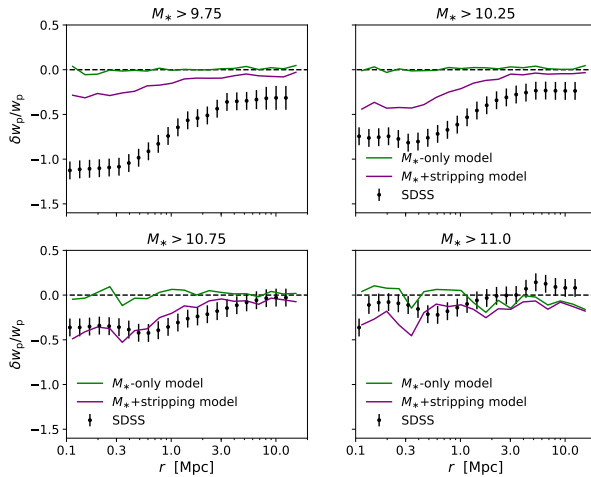


**Figure 7. Impact of tidal stripping.** In all panels, the axes and points with error bars are the same as in Figure 5. The solid green curves show the prediction of the  $M_*$ -based model, which is in gross tension with the data due to satellites having the same size as centrals of the same mass. The solid purple curves show results for a model in which satellites lose mass after infall in a manner similar to what is seen in high-resolution hydrodynamical simulations, as described in §3.2.3. This produces satellites that are smaller than centrals, but the effect is too mild to correctly capture the observed clustering. Evidently, satellite-specific mass stripping plays a sub-dominant role in setting the relative size of centrals and satellites.

quantities such as  $M_{\text{halo}}$ . In the case of *Halotools*, this transforms a cosmological simulation into a synthetic galaxy catalog that can be directly compared with observations. This enables a richer quantitative study of modeling hypotheses relative to backwards modeling. For example, Figure 5 shows how forward modeling allows us to exploit galaxy clustering measurements to quantitatively test whether  $M_{\text{halo}}$  or  $M_*$  is the statistical regulator of galaxy size. The ability disentangle coupled variables such as  $M_*$  and  $M_{\text{halo}}$  is just one example of this advantage of forward modeling. Another example is illustrated in Figure 6, in which we explore the role of splash-back halos in setting galaxy size. In our forward modeling approach, this is entirely straightforward; in backwards modeling, such an investigation would not even be possible without introducing additional modeling ingredients.

Backwards modeling the galaxy-halo connection is useful for generating hypotheses and motivating functional forms. Forward modeling becomes necessary when the problem at hand becomes encumbered by multiple relevant variables, as is the case with galaxy size. Forward modeling also makes it possible to conduct rigorous Bayesian inference, which we consider to be the next natural step in the progression described here (see §5.4 for further discussion).

## 5.2 Relation to Previous Work

Backwards modeling methods have been used extensively in the literature to gain insight into the relationship between galaxy mass, size, and environment. Broadly

speaking, such studies proceed by using a galaxy group catalog to classify observed galaxies as centrals or satellites, and estimate their halo mass. Employing such methods, several analyses of the Yang et al. (2005) group catalog have found that the  $M_* - R_{1/2}$  relation of early-type galaxies exhibits weak, if any, environmental dependence (Huertas-Company et al. 2013; Shankar et al. 2014).

A direct comparison to this finding is not possible because the conclusions drawn here pertain to  $M_*$ -limited galaxy samples. As discussed in Spindler & Wake (2017), it is entirely possible that size differences between centrals and satellites of the same mass can be accounted for by mutual covariance with an additional variable such as star formation rate or morphological type (see also Lilly & Carollo 2016, for an explicit demonstration of this scenario). In particular, suppose that centrals and satellites of the same mass have different early-type fractions as indicated in Weinmann et al. (2006), and that early- and late-type galaxies exhibit universal, but distinct,  $M_* - R_{1/2}$  relations. In such a case, centrals would be larger than satellites of the same mass, even though *early-type centrals* would have the same sizes as *early-type satellites*.

As discussed in §5.4, we are currently pursuing follow-up work in which we jointly model morphological type together with galaxy size. We consider forward modeling methods to be a requisite for progress on this issue, not only to properly handle the multi-dimensional nature of the problem, but also to rigorously treat systematic errors that plague inference based on galaxy group catalogs (see Campbell et al. 2015, for a thorough discussion).

Our approach is closely aligned with the methods used in Somerville et al. (2017), who studied the empirical modeling features that are necessary to recover the tight scatter in the observed  $\langle R_{1/2} | M_* \rangle$  relation. By building models where  $R_{1/2}$  is set by halo spin  $\lambda_{\text{halo}}$ , the authors in Somerville et al. (2017) found that the level of intrinsic scatter about  $\langle \lambda_{\text{halo}} | M_{\text{halo}} \rangle$  in dark matter halos is at least as large as the scatter about  $\langle R_{1/2} | M_* \rangle$  seen in observed galaxies. Since the latter necessarily receives an additional contribution from measurement error, this implies some tension with the common semi-analytic modeling assumption that  $\lambda_{\text{halo}}$  scales with  $R_{1/2}$ . As noted in Somerville et al. (2017), tension in the level of scatter cannot be used to directly test the  $\lambda_{\text{halo}} \propto R_{1/2}$  assumption because the physical motivation for this correlation is largely limited to disk galaxies (Mo et al. 1998). This tension is not present in our approach for the reason that the level of scatter is simply a modeling parameter in our approach, and we make no attempt to uncover the physical origin of this scatter. However, our fiducial value choice was motivated by Somerville et al. (2017), and in the ongoing follow-up work discussed in §5.4 we will systematically test the large-scale structure implications of the assumption that  $\lambda_{\text{halo}} \propto R_{1/2}^{\text{disk}}$ .

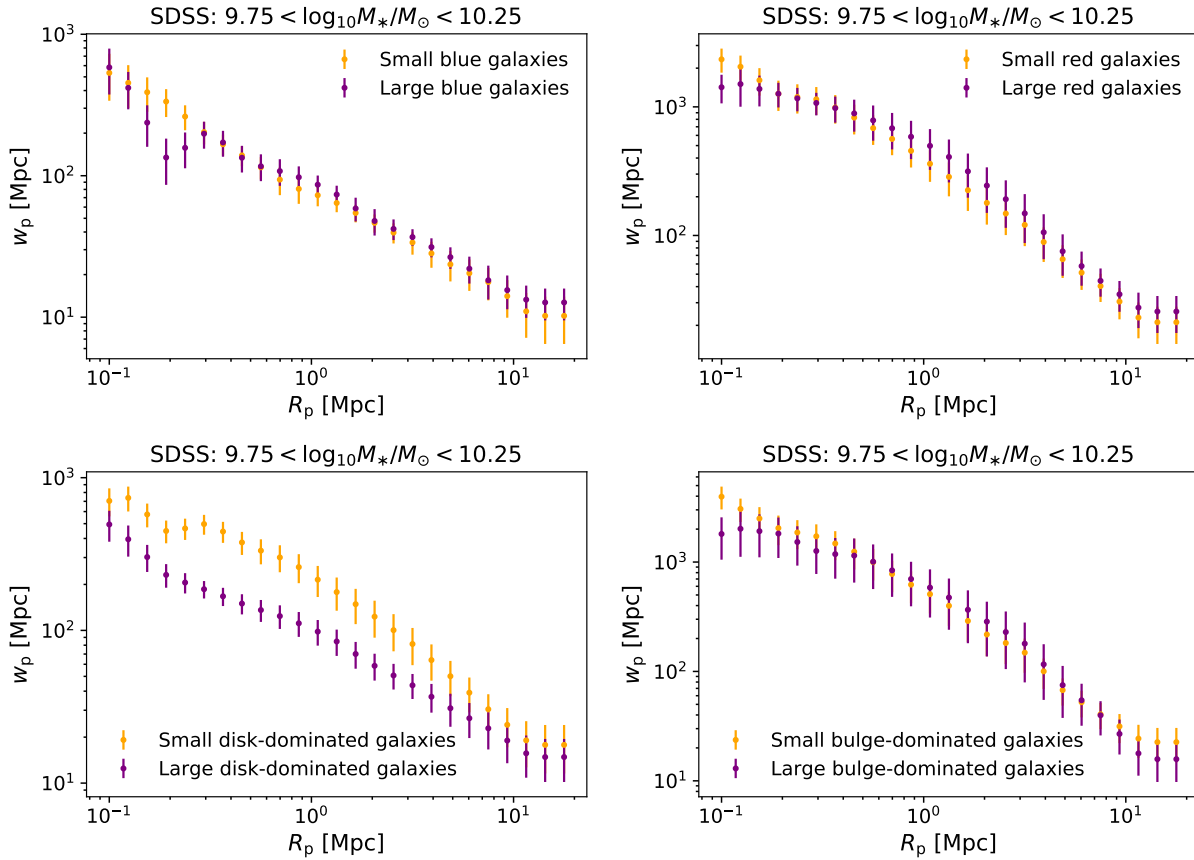


**Figure 8. Distinct  $R_{1/2}$ –dependence of clustering for color- or morphology-selected galaxy samples.** All panels show the clustering of galaxies in the same bin of stellar mass:  $10^{9.75} < M_*/M_\odot < 10^{10.25}$ . In the *upper left* panel, we first select blue galaxies based on  $g - r < 0.6$ , and subsequently compute  $\langle R_{1/2} | M_* \rangle_{\text{median}}$  of the *color-selected sample*. This results in identical stellar mass function for large and small blue galaxy samples, in analogy to the left panel of Figure 1. The *upper right* panel shows results of the same procedure for “red” galaxies, defined by  $g - r > 0.6$ . The top two panels show that for color-selected samples, the magnitude of the  $R_{1/2}$ –dependence of clustering is dramatically reduced, and changes sign, relative to  $M_*$ –complete samples. Using the Meert et al. (2015) measurements of the disk/bulge decomposition of the 2d  $r$ –band luminosity profile  $L_r$ , the bottom left panel shows analogous results for disk-dominated galaxies defined by  $L_r^{\text{bulge}} < L_r^{\text{tot}}/4$ ; the bottom right panel shows results for bulge-dominated galaxies defined by  $L_r^{\text{disk}} < L_r^{\text{tot}}/4$ .

### 5.3 Implications for Satellite Evolution

### 5.4 Future Directions for Empirical Modeling of Galaxy Size

#### 5.4.1 Jointly modeling $\langle M_* | M_{\text{halo}} \rangle$

#### 5.4.2 Jointly modeling morphology

## 6 CONCLUSIONS

We have presented new measurements of the dependence of galaxy clustering upon galaxy size, and used *Halotools* to identify the basic ingredients that influence the signal. We conclude with a brief summary of our primary findings:

- (i) Small galaxies cluster more strongly than large galaxies of the same stellar mass. Differences between the clustering of small and large galaxies increase on small scales  $R \lesssim 1\text{Mpc}$ , and decrease with stellar mass.
- (ii) The most important ingredient influencing this signal is the relative size of central and satellite galaxies. The magnitude, scale-dependence, and  $M_*$ –dependence

of  $R_{1/2}$ –dependent clustering provides strong evidence that satellite galaxies are smaller than central galaxies of the same halo mass.

(iii) A simple empirical model in which  $R_{1/2}$  is set by halo  $R_{\text{vir}}$  at the time of peak halo mass exhibits a clustering signal that is strikingly similar to that seen in SDSS.

(iv) Models in which  $R_{1/2}$  is regulated by  $M_*$ , rather than  $M_{\text{halo}}$ , are grossly discrepant with the observed clustering signal, even when accounting for satellite mass stripping.

(v) Taken together, our findings indicate that satellite-specific processes play a sub-dominant role in setting the relative size of centrals and satellites, which instead appears to be largely predetermined at the time of satellite infall.

Our results can be treated as a boundary condition for more complex and fine-grained models of galaxy size, such as semi-analytic models and hydrodynamical simulations. We view the present work as a pilot study that motivates a Bayesian inference program to tightly con-

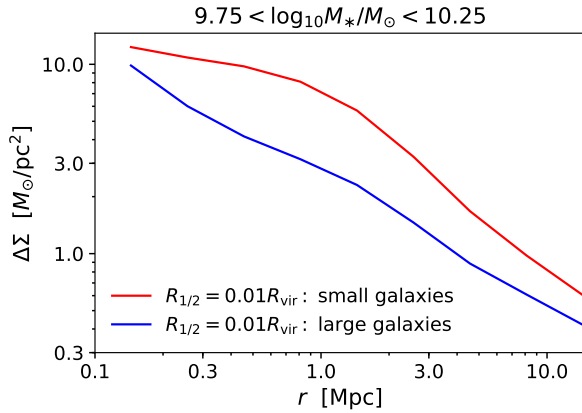


**Figure 9. Prediction for  $R_{1/2}$ -dependence of galaxy lensing.** Using the  $R_{\text{vir}}$ -based model described in §3.2.2, we make predictions for as-yet-unseen measurements of the  $R_{1/2}$ -dependence of galaxy lensing of  $M_*$ -complete samples. To date, the  $R_{1/2}$ -dependence of  $\Delta\Sigma$  has only been measured for color-selected samples (Charlton et al. 2017), in which the reverse is true: for both blue and red samples,  $\Delta\Sigma$  of small galaxies is (weakly) suppressed relative to large galaxies. As a generic consequence of satellites being smaller than centrals of the same mass, we predict that the analogous measurement for  $M_*$ -complete samples will show  $\Delta\Sigma$  of small galaxies to be much stronger relative to large galaxies of the same stellar mass.

strain the galaxy size-halo connection with forward modeling techniques, in direct analogy to the literature on the stellar-to-halo-mass relation. Our publicly available python code provides a simple means for cosmological surveys to generate synthetic galaxy populations with realistic sizes across the cosmic web.

## ACKNOWLEDGMENTS

APH thanks John Baker for the *Toejam & Earl* soundtrack. Thanks also to Frank van den Bosch, Doug Watson, and Risa Wechsler for thoughtful feedback at various stages of the development of this work, and to Faustin Carter and Sebastian Bocquet for sharing their python expertise.

We thank the **Astropy** developers for the package-template (Astropy Collaboration et al. 2013), and **NumPy** (Van Der Walt et al. 2011), **SciPy** (Jones et al. 2016), **IPython**, **Matplotlib**, and **GitHub** for their extremely useful free software.

This research was supported in part by the National Science Foundation under Grant No. NSF PHY11-25915. Work done at Argonne National Laboratory was supported under the DOE contract DE-AC02-06CH11357.

## REFERENCES

Ahn C. P., Alexandroff R., Allende Prieto C., Anders F., Anderson S. F., Anderton T., Andrews B. H., Aubourg É., Bailey S., Bastien F. A., et al. 2014, *ApJS*, 211, 17

Astropy Collaboration Robitaille T. P., Tollerud E. J., Greenfield P., Droettboom M., Bray E., Aldcroft T., et al., 2013, *AAP*, 558, A33  
 Behroozi P. S., Wechsler R. H., Wu H.-Y., 2013, *ApJ*, 762, 109  
 Behroozi P. S., Wechsler R. H., Wu H.-Y., Busha M. T., Klypin A. A., Primack J. R., 2013, *ApJ*, 763, 18  
 Behroozi P. S., Zhu G., Ferguson H. C., Hearin A. P., Lotz J., Silk J., Kassin S., Lu Y., Croton D., Somerville R. S., Watson D. F., 2015, *MNRAS*, 450, 1546  
 Berlind A. A., Frieman J., Weinberg D. H., et al., 2006, *ApJS*, 167, 1  
 Bernardi M., Meert A., Sheth R. K., Vikram V., Huertas-Company M., Mei S., Shankar F., 2013, *MNRAS*, 436, 697  
 Bernardi M., Meert A., Vikram V., Huertas-Company M., Mei S., Shankar F., Sheth R. K., 2014, *MNRAS*, 443, 874  
 Bottrell C., Torrey P., Simard L., Ellison S. L., 2017, *MNRAS*, 467, 2879  
 Brinchmann J., Charlot S., White S. D. M., Tremonti C., Kauffmann G., Heckman T., Brinkmann J., 2004, *MNRAS*, 351, 1151  
 Bryan G. L., Norman M. L., 1998, *ApJ*, 495, 80  
 Campbell D., van den Bosch F. C., Hearin A., Padmanabhan N., Berlind A., Mo H. J., Tinker J., Yang X., 2015, *MNRAS*, 452, 444  
 Campbell D., van den Bosch F. C., Padmanabhan N., Mao Y.-Y., Zentner A. R., Lange J. U., Jiang F., Villarreal A., 2017, *ArXiv:1705.06347*  
 Charlton P. J. L., Hudson M. J., Balogh M. L., Khatri S., 2017, *MNRAS*, 472, 2367  
 Croton D. J., 2013, *PASA*, 30, e052  
 Dutton A. A., van den Bosch F. C., Faber S. M., Simard L., Kassin S. A., Koo D. C., Bundy K., Huang J., Weiner B. J., Cooper M. C., Newman J. A., Mozena M., Koekemoer A. M., 2011, *MNRAS*, 410, 1660  
 Guo Q., White S., 2014, *MNRAS*, 437, 3228  
 Guo Y., McIntosh D. H., Mo H. J., Katz N., Van Den Bosch F. C., Weinberg M., Weinmann S. M., Pasquali A., Yang X., 2009, *MNRAS*, 398, 1129  
 Hopkins P. F., Bundy K., Croton D., Hernquist L., Keres D., Khochfar S., Stewart K., Wetzel A., Younger J. D., 2010, *ApJ*, 715, 202  
 Huang K.-H., Fall S. M., Ferguson H. C., van der Wel A., Grogin N., Koekemoer A., Lee S.-K., Pérez-González P. G., Wuyts S., 2017, *ApJ*, 838, 6  
 Huang S., Ho L. C., Peng C. Y., Li Z.-Y., Barth A. J., 2013, *ApJ*, 766, 47  
 Huertas-Company M., Mei S., Shankar F., Delaye L., Raichoor A., Covone G., Finoguenov A., Kneib J. P., Le F. O., Povic M., 2013, *MNRAS*, 428, 1715  
 Huertas-Company M., Shankar F., Mei S., Bernardi M., Aguerri J. A. L., Meert A., Vikram V., 2013, *ApJ*, 779, 29  
 Jiang F., van den Bosch F. C., 2014, *ArXiv e-prints*  
 Jones E., Oliphant T., Peterson P., et al., 2001-2016, <http://www.scipy.org>  
 Kauffmann G., Heckman T. M., White S. D. M., et al., 2003, *MNRAS*, 341, 33  
 Kawamata R., Ishigaki M., Shimasaku K., Oguri M., Ouchi M., 2015, *ApJ*, 804, 103



Khochfar S., Silk J., 2006, *ApJL*, 648, L21  
 Klypin A. A., Trujillo-Gomez S., Primack J., 2011, *ApJ*, 740, 102  
 Kravtsov A. V., 2013, *ApJL*, 764, L31  
 Lange R., Driver S. P., Robotham A. S. G., et al., 2015, *MNRAS*, 447, 2603  
 Lilly S. J., Carollo C. M., 2016, *ApJ*, 833, 1  
 LSST Science Collaboration Abell P. A., Allison J., Anderson S. F., Andrew J. R., Angel J. R. P., Armus L., Arnett D., Asztalos S. J., Axelrod T. S., et al. 2009, *ArXiv e-prints*  
 Meert A., Vikram V., Bernardi M., 2013, *MNRAS*, 433, 1344  
 Meert A., Vikram V., Bernardi M., 2015, *MNRAS*, 446, 3943  
 Mo H. J., Mao S., White S. D. M., 1998, *MNRAS*, 295, 319  
 Planck Collaboration Ade P. A. R., Aghanim N., Arnaud M., Ashdown M., Aumont J., Baccigalupi C., Banday A. J., Barreiro R. B., Bartlett J. G., et al. 2016, *AAP*, 594, A13  
 Riebe K., Partl A. M., Enke H., Forero-Romero J., Gottlöber S., Klypin A., Lemson G., Prada F., Primack J. R., Steinmetz M., Turchaninov V., 2013, *Astronomische Nachrichten*, 334, 691  
 Robertson B. E., Banerji M., Cooper M. C., Members of the LSST Galaxies Science Collaboration 2017, *ArXiv e-prints*  
 Rodríguez-Puebla A., Behroozi P., Primack J., Klypin A., Lee C., Hellinger D., 2016, *MNRAS*, 462, 893  
 Rykoff E. S., Rozo E., Busha M., et al., 2014, *ApJ*, 785, 104  
 Shankar F., Mei S., Huertas-Company M., Moreno J., Fontanot F., Monaco P., Bernardi M., Cattaneo A., Sheth R., Licitra R., Delaye L., Raichoor A., 2014, *MNRAS*, 439, 3189  
 Shen S., Mo H. J., White S. D. M., Blanton M. R., Kauffmann G., Voges W., Brinkmann J., Csabai I., 2003, *MNRAS*, 343, 978  
 Shibuya T., Ouchi M., Harikane Y., 2015, *ApJS*, 219, 15  
 Sinha M., Garrison L., , 2017, *Corrfunc: Blazing fast correlation functions on the CPU*, *Astrophysics Source Code Library*  
 Smith R., Choi H., Lee J., Rhee J., Sanchez-Janssen R., Yi S. K., 2016, *ApJ*, 833, 109  
 Somerville R. S., Behroozi P., Pandya V., et al., 2017, *ArXiv e-prints*  
 Spindler A., Wake D., 2017, *MNRAS*, 468, 333  
 Trujillo I., Rudnick G., Rix H.-W., Labbé I., Franx M., Daddi E., van Dokkum P. G., Förster Schreiber N. M., Kuijken K., Moorwood A., Röttgering H., van der Wel A., van der Werf P., van Starkenburg L., 2004, *ApJ*, 604, 521  
 Van Der Walt S., Colbert S. C., Varoquaux G., 2011, *ArXiv:1102.1523*  
 van der Wel A., Franx M., van Dokkum P. G., et al., 2014, *ApJ*, 788, 28  
 Vikram V., Wadadekar Y., Kembhavi A. K., Vijayagovindan G. V., 2010, *MNRAS*, 409, 1379  
 Weinmann S. M., van den Bosch F. C., Yang X., Mo H. J., 2006, *MNRAS*, 366, 2

Yang X., Mo H. J., Jing Y. P., van den Bosch F. C., 2005, *MNRAS*, 358, 217  
 Yang X., Mo H. J., van den Bosch F. C., Jing Y. P., 2005, *MNRAS*, 356, 1293  
 Zhang Y., Yang X., 2017, *ArXiv e-prints*

## APPENDIX: TREATMENT OF DISRUPTED SUBHALOS

We use an extension of **Consistent Trees** that models the evolution of subhalos after disruption. The phase space evolution of disrupted subhalos is approximated by following a point mass evolving in the host halo potential according to the orbital parameters of the subhalo at the time of disruption; the evolution of subhalo mass and circular velocity is approximated using the semi-analytic model presented in Jiang & van den Bosch (2014). We then use the **orphans** program in **UniverseMachine** to walk through all the Bolshoi-Planck **hlist** files, yielding the main progenitor information of every subhalo that was ever identified by **Consistent Trees**.

Since it is likely that some portion of these disrupted subhalos should be populated with model galaxies (Guo & White 2014; Campbell et al. 2017), in our initial application of deconvolution abundance matching we derive the  $M_* - -M_{\text{peak}}$  relation using *all* subhalos, including those that may be disrupted. We then apply a selection function to the disrupted subhalos, so that a fraction of these objects will host galaxies in our mock universe. We refer to this as the *orphan selection function*,  $\mathcal{F}_{\text{orphan}}$ , which we consider to be an integral component of our application of abundance matching.

Since a rigorous calibration of  $\mathcal{F}_{\text{orphan}}$  is beyond the scope of the present work, we instead opt for a simple parameterization that yields reasonably accurate recovery of the galaxy clustering signal observed in SDSS. We model  $\mathcal{F}_{\text{orphan}} = \mathcal{F}_{\text{orphan}}(M_{\text{peak}}, M_{\text{host}})$ , where  $M_{\text{peak}}$  is the peak mass of the disrupted subhalo, and  $M_{\text{host}}$  is the present-day virial mass of its  $z = 0$  host halo. For the  $M_{\text{peak}}$ -dependence, we select 50% of disrupted subhalos with  $M_{\text{peak}} = 10^{11} M_{\odot}$ , 0% of subhalos with  $M_{\text{peak}} = 10^{13} M_{\odot}$ , linearly interpolating in  $\log M_{\text{peak}}$  for intermediate values of  $M_{\text{peak}}$ . At each  $M_{\text{peak}}$ , the selection of disrupted halos is not random; instead, we preferentially select the subhalos with larger  $M_{\text{host}}$ , which we intend to offset the increased difficulty of subhalo-finding algorithms to identify subhalos with especially small values of  $\mu \equiv M_{\text{peak}}/M_{\text{host}}$ .